

Tunable Gaussian Entanglement in Cavity-Magnon Optomechanics

Ming-Yue Liu,¹ Xian-Xian Huang,¹ Jiaojiao Chen,^{2,*} and Wei Xiong^{1,†}

¹*Department of Physics, Wenzhou University, Zhejiang 325035, China*

²*School of Physics and Optoelectronics Engineering, Anhui University, Hefei 230601, China*

(Dated: April 24, 2024)

Cavity optomechanics, providing an inherently nonlinear interaction between photons and phonons, have shown enomorous potential in generating macroscopic quantum entanglement. Here we propose to realize diverse bipartite and tripartite entanglement in cavity-magnon optomechanics. By introducing magnons to standard cavity optomechanics, not only tunable optomechanical entanglement and magnon-magnon entanglement can be achieved, but also flexible tripartite entanglement including magnon-photon-phonon entanglement, magnon-magnon-photon and -phonon entanglement can be generated. Moreover, optimal bipartite and tripartite entanglement can be achieved by tuning parameters. We further show that all entanglement can be enhanced via engineering the magnon-photon coupling, and is proven to be robust against the bath temperature within the survival temperature. Besides, we find that the optomechanical entanglement can be protected or restored by bad magnons with large decay rate, while other entanglement is severely reduced. The results indicate that our proposal provides a novel avenue to explore and control tunable macroscopic quantum effects in hybrid cavity-magnon optomechanics.

I. INTRODUCTION

Magnons [1, 2], quanta of collective spin-wave excitations in magnetically ordered materials like yttrium iron garnet (YIG), have garnered considerable interest in quantum physics and condensed matter physics [3–8]. With unique properties such as high spin density and low energy loss [9–11], diverse novel phenomena including strong [9–12] and ultrastrong coupling [13–15], qubit-magnon coupling [16], magnon dark modes and gradient memory [17], magnon Kerr effect [18], spin current manipulation [19], exceptional points [20–23], axion detection [24–26], superradiant phase transition [27], dissipative coupling [28, 29], and strong spin coupling [30–36]. Recently, special attention has been paid to macroscopic quantum entanglement associated with magnons [37–45]. This is because it is crucial for understanding the classical-quantum boundary [46] and can be regarded as an important resource for quantum information science [47]. However, to produce such macroscopic entanglement, nonlinear effects are always pre-required [48]. The extensively explored cavity optomechanics [49–56], hybridized by photons in a cavity mode weakly coupled to phonons in a mechanical resonator through radiation pressure [57], can provide the natural nonlinearity for investigating optomechanical entanglement [58] and other intriguing effects such as sensing [59–61], ground-state cooling [62–71], squeezed light generation [70–77], nonreciprocity [78–86], optomechanically induced transparency [87–96], coupling enhancement [97–102], multistability [103–106], and high-order exceptional points [107–109]. This indicates that combination of magnonics and optomechanics is a potential

path to investigate macroscopic magnon entanglement.

Owing to the strong photon-magnon coupling in planar [9] and 3D cavities [10–12], hybridizing magnons with optomechanics to form cavity-magnon optomechanics becomes feasible [31, 39, 40, 110, 111] for utilizing their individual advantages. In this work, we propose to generate diverse bipartite and tripartite entanglement in hybrid cavity-magnon optomechanics. Compared to the standard cavity optomechanics, the optomechanical entanglement can be adjusted flexibly by the introduced magnons in the Kittle mode of a single sphere. Specifically, the optimal optomechanical entanglement can be predicted by tuning the detuning of the Kittle mode from the driving field to be resonant with the mechanical mode (i.e., $\Delta_m = \omega_b$). But when we tune this detuning to be anti-resonant with the mechanical mode (i.e., $\Delta_m = -\omega_b$), the optomechanical entanglement is weakest, while the magnon-photon entanglement, the magnon-phonon, as well as the magnon-photon-phonon entanglement are approximately optimal. These entanglement can be further enhanced by engineering the coupling between magnons and photons. In addition, the tunable magnon-magnon entanglement and the tripartite entanglement including the magnon-magnon-photon entanglement and the magnon-magnon-phonon entanglement can also be generated in the proposed cavity-magnon optomechanics with two spheres. Tuning one Kittle mode to be resonant with the mechanical mode (i.e., $\Delta_1 = \omega_b$), while the other to be anti-resonant with the mechanical mode (i.e., $\Delta_2 = -\omega_b$), or vice versa, the optimal magnon-magnon entanglement is predicted, and its value approximately equals to half the optomechanical entanglement. But to have optimal magnon-magnon-photon and -phonon entanglement, two Kittle modes are needed to be resonant (i.e., $\Delta_1 = \Delta_2$). We further show that the optomechanical entanglement can be protected or restored by using bad magnons with large decay rate, but the magnon-magnon entanglement

*jjchenphys@hotmail.com

†xiongweiphys@wzu.edu.cn

as well as the magnon-magnon-photon and -phonon entanglement are severely reduced. Besides, the bath temperature effect on these entanglement are also investigated. We find that for the weaker magnon-photon coupling (i.e., $g_m < G$), the stronger optomechanical entanglement than that of the magnon-magnon entanglement can be obtained within the survival temperature, but the situation is reversed when the magnon-photon coupling becomes comparable with the optomechanical coupling (i.e., $g_m \approx G$). Moreover, the survival temperature of the magnon-magnon entanglement is more robust against the magnon-photon coupling than that of the optomechanical entanglement. For the tripartite entanglement, we show that the magnon-magnon-phonon entanglement is stronger than the magnon-magnon-photon entanglement within their survival temperature, owing to the mechanical cooling. All achieved entanglement exhibit robust against the bath temperature. Our proposal opens an alternative path to study tunable macroscopic quantum effect in hybrid cavity-magnon optomechanics.

This rest paper is organized as follows: In Sec. II, the model is described and the entanglement quantification is given. Then in Sec. III, we study optomechanical entanglement mediated by magnons in the proposed cavity-magnon optomechanics, where only a single sphere is considered. In Sec. IV, tunable magnon-magnon entanglement induced by the optomechanical interface is investigated via examining the effect of system parameters. In Sec. V, we further study tripartite entanglement including magnon-magnon-photon and magnon-magnon-phonon entanglement. Finally, a conclusion is given in Sec. VI.

II. MODEL AND ENTANGLEMENT QUANTIFICATION

A. Model

We consider a hybrid cavity-magnon optomechanics consisting of a mechanical resonator weakly coupled to a cavity containing two separated YIG spheres, as depicted in Fig. 1(a). The magnons in the Kittle modes of two spheres are strongly coupled to the photons in the cavity mode with the uniform coupling strength $g_1 = g_2 = g_m$. By imposing an external field, with the frequency ω_0 and the amplitude Ω , to the cavity, the Hamiltonian of the proposed hybrid system with respect to ω_0 , can be given by (setting $\hbar = 1$)

$$H_{\text{sys}} = H_{\text{OM}} + \sum_{j=1,2} H_{\text{CM}}^{(j)} + i\Omega (a^\dagger - a), \quad (1)$$

where $H_{\text{OM}} = \Delta_a a^\dagger a + \frac{\omega_b}{2} (q^2 + p^2) + g_0 a^\dagger a q$ denotes the Hamiltonian of the standard cavity optomechanics, describing the interaction between the cavity mode and the mechanical mode via the radiation pressure, with the single-photon optomechanical coupling strength g_0 .

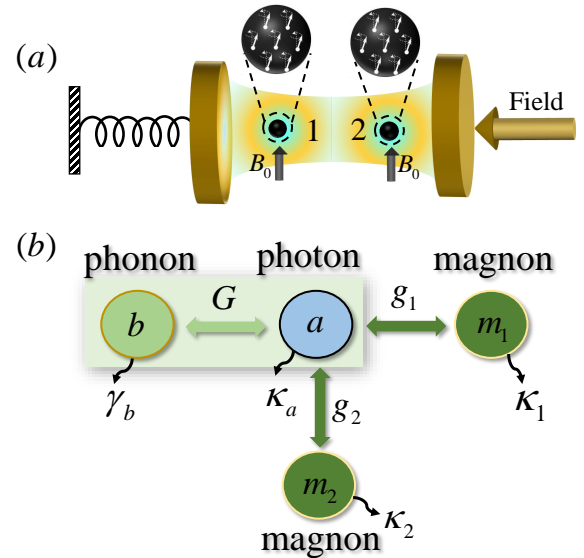


FIG. 1: (a) Schematic diagram of the proposed cavity-magnon optomechanics. It consists of two YIG spheres placed in a cavity containing two separated YIG spheres, as depicted in Fig. 1(a). The magnons in the Kittle modes of two spheres are strongly coupled to the photons in the cavity mode with the uniform coupling strength $g_1 = g_2 = g_m$. By imposing an external field, with the frequency ω_0 and the amplitude Ω , to the cavity, the Hamiltonian of the proposed hybrid system with respect to ω_0 , can be given by (setting $\hbar = 1$)

$\Delta_a = \omega_a - \omega_0$, with ω_a being the frequency of the cavity mode, is the frequency detuning of the cavity mode from the driving field, and ω_b is the frequency of the mechanical mode. The Hamiltonian $H_{\text{CM}}^{(j)} = \Delta_j m_j^\dagger m_j + g_j (m_j a^\dagger + m_j^\dagger a)$ characterizes the interaction between the cavity mode and the Kittle mode of the j th sphere. $\Delta_j = \omega_j - \omega_0$ is the frequency detuning of the Kittle mode of the j th sphere from the driving field. The creation (annihilation) operators of the cavity mode and the Kittle mode of the j th sphere are denoted by a^\dagger (a) and m_j^\dagger (m_j), respectively. q and p are dimensionless position and momentum quadratures of the mechanical mode.

B. Quantum Langevin equation

By taking input noises and dissipations into account, the dynamics of the proposed system can be governed by the quantum Langevin equations, i.e.,

$$\begin{aligned} \dot{q} &= \omega_b p, \\ \dot{p} &= -\omega_b q - g_0 a^\dagger a - \gamma_b p + \xi, \\ m_j &= -(\kappa_j + i\Delta_j) m_j - i g_j a + \sqrt{2\kappa_j} \zeta_j, \\ \dot{a} &= -(\kappa_a + i\Delta_a) a - i g_0 a q - i g_j m_j + \Omega + \sqrt{2\kappa_a} \mu, \end{aligned} \quad (2)$$

where κ_a , κ_j , and γ_b are the decay rates of the cavity mode, the Kittle mode of the j th sphere, and the mechanical mode, respectively. For simplicity, we assume that the Kittle modes of two spheres have the identical decay rate $\kappa_1 = \kappa_2 = \kappa_m$ below. μ , ζ_j and ξ are the vacuum input noise operators for the cavity mode, the mechanical mode, and the Kittle mode of the j th sphere, having the zero mean values $\langle \mu \rangle = \langle \zeta_j \rangle = \langle \xi \rangle = 0$. Under the Markovian approximation, two-time correlation functions of these input noise operators are

$$\begin{aligned}\langle \mu(t)\mu^\dagger(t') \rangle &= (\bar{n}_a + 1)\delta(t - t'), \\ \langle \mu^\dagger(t)\mu(t') \rangle &= \bar{n}_a\delta(t - t'), \\ \langle \zeta_j(t)\zeta_j^\dagger(t') \rangle &= (\bar{n}_j + 1)\delta(t - t'), \\ \langle \zeta_j^\dagger(t)\zeta_j(t') \rangle &= \bar{n}_j\delta(t - t'), \\ \langle \xi(t)\xi(t') + \xi(t')\xi(t) \rangle &\simeq 2\gamma_b(2\bar{n}_b + 1)\delta(t - t'),\end{aligned}\quad (3)$$

where $\bar{n}_\sigma = [\exp(\hbar\omega_\sigma/k_B T) - 1]^{-1}$ ($\sigma = a, b, j$) is the mean thermal excitation number, with k_B being the Boltzmann constant and T the bath temperature.

In fact, Eq. (2) can be linearized when the external driving field is strong. For this, we first rewrite the operator $O = \langle O \rangle + \delta O$ ($O = q, p, a, m_j$), where $\langle O \rangle$ is the steady-state value and δO is the fluctuation operator. Then we substitute the redefined operator O into Eq. (2) and neglect the high-order fluctuation terms, resulting in

$$\begin{aligned}\dot{\delta q} &= \omega_b \delta p, \\ \dot{\delta p} &= -\omega_b \delta q - (G^* \delta a + G \delta a^\dagger)/\sqrt{2} - \gamma_b \delta p + \xi, \\ \dot{\delta m}_j &= -(\kappa_j + i\Delta_j)\delta m_j - ig_j \delta a + \sqrt{2\kappa_j}\zeta_j, \\ \dot{\delta a} &= -(\kappa_a + i\tilde{\Delta}_a)\delta a - iGq/\sqrt{2} - ig_j \delta m_j + \sqrt{2\kappa_a}\mu,\end{aligned}\quad (4)$$

where $\tilde{\Delta}_a = \Delta_a + g_0\langle q \rangle$ is the effective frequency detuning, induced by the displacement of the mechanical mode, and $G = \sqrt{2}g_0\langle a \rangle$ is the effectively enhanced optomechanical coupling strength between the cavity mode and the mechanical mode by the factor $\langle a \rangle$. The steady-state values $\langle O \rangle$ in Eq. (4) are given by $\langle O \rangle = 0$. Specifically, $\langle p \rangle = 0$, $\langle q \rangle = -g_0|\langle a \rangle|^2/\omega_b$, $\langle m_j \rangle \approx -g_j\langle a \rangle/\Delta_j$, and $\langle a \rangle \approx i\Omega/(g_j^2/\Delta_j - \tilde{\Delta}_a)$, where $|\Delta_j|, |\tilde{\Delta}_a| \gg \kappa_j, \kappa_a$

are taken. Experimentally, these conditions can be easily achieved by tuning the frequency of the driving field. Also, the value of $\langle a \rangle$ can be real via tuning the initial phase of the strong driving field. Hereafter, we assume $\langle a \rangle$ to be real for simplicity. Thus, the effective Hamiltonian of the linearized hybrid system can be written as

$$\begin{aligned}H_{\text{eff}} &= \tilde{\Delta}_a a^\dagger a + \frac{\omega_b}{2} (q^2 + p^2) + \frac{G}{\sqrt{2}}(a + a^\dagger)q \\ &\quad + \sum_{j=1,2} \Delta_j m_j^\dagger m_j + g_j(m_j a^\dagger + a m_j^\dagger),\end{aligned}\quad (5)$$

which effectively describes the interaction among the cavity mode, the mechanical mode, and the Kittle modes, as illustrated in Fig. 1(b). Notably, all parameters in the Hamiltonian (5) are adjustable except for the mechanical frequency ω_b . The fluctuation symbol “ δ ” is omitted for convenience.

C. Covariance matrix

By further defining fluctuation quadratures of the Kittle and the cavity modes as

$$\begin{aligned}x_j &= (m_j + m_j^\dagger)/\sqrt{2}, \quad y_j = i(m_j^\dagger - m_j)/\sqrt{2}, \\ x_a &= (a + a^\dagger)/\sqrt{2}, \quad y_a = i(a^\dagger - a)/\sqrt{2},\end{aligned}\quad (6)$$

and the associated input noise operators as

$$\begin{aligned}X_j &= (\zeta_j + \zeta_j^\dagger)/\sqrt{2}, \quad Y_j = i(\zeta_j^\dagger - \zeta_j)/\sqrt{2}, \\ X_\mu &= (\mu + \mu^\dagger)/\sqrt{2}, \quad Y_\mu = i(\mu^\dagger - \mu)/\sqrt{2},\end{aligned}\quad (7)$$

the dynamics in Eq. (4) can be equivalently written as the matrix form,

$$\dot{u}(t) = Au(t) + n(t), \quad (8)$$

where $u(t) = [x_1, y_1, x_2, y_2, x_a, y_a, q, p]^T$ is the vector operator of the system, $n(t) = [\sqrt{2\kappa_1}X_1, \sqrt{2\kappa_1}Y_1, \sqrt{2\kappa_2}X_2, \sqrt{2\kappa_2}Y_2, \sqrt{2\kappa_a}X_\mu, \sqrt{2\kappa_a}Y_\mu, 0, \xi]^T$ is the vector operator of the input noise, and

$$A = \begin{pmatrix} -\kappa_1 & \Delta_1 & 0 & 0 & 0 & g_1 & 0 & 0 \\ -\Delta_1 & -\kappa_1 & 0 & 0 & -g_1 & 0 & 0 & 0 \\ 0 & 0 & -\kappa_2 & \Delta_2 & 0 & g_2 & 0 & 0 \\ 0 & 0 & -\Delta_2 & -\kappa_2 & -g_2 & 0 & 0 & 0 \\ 0 & g_1 & 0 & g_2 & -\kappa_a & \tilde{\Delta}_a & 0 & 0 \\ -g_1 & 0 & -g_2 & 0 & -\tilde{\Delta}_a & -\kappa_a & -G & 0 \\ 0 & 0 & 0 & 0 & 0 & 0 & 0 & \omega_b \\ 0 & 0 & 0 & 0 & -G & 0 & -\omega_b & \gamma_b \end{pmatrix} \quad (9)$$

is the drift matrix. According to the Routh-Hurwitz

criteria[112, 113], the system is stable only when all the

eigenvalues of A have negative real parts. The stability is ensured numerically in the following.

Since the input quantum noises are zero-mean quantum Gaussian noises, the quantum steady state for the fluctuations is a zero-mean continuous variable Gaussian state, fully characterized by an 8×8 covariance matrix $\mathcal{V}_{lk}(t) = \frac{1}{2} \langle u_l(t)u_k(t') + u_k(t')u_l(t) \rangle$ ($l, k = 1, 2, \dots, 8$). The matrix \mathcal{V} can be obtained by directly solving the Lyapunov equation[114]

$$A\mathcal{V} + \mathcal{V}A^T + \mathcal{D} = 0, \quad (10)$$

where $\mathcal{D} = \text{diag}[\kappa_1(2\bar{n}_1 + 1), \kappa_1(2\bar{n}_1 + 1), \kappa_2(2\bar{n}_2 + 1), \kappa_2(2\bar{n}_2 + 1), \kappa_a(2\bar{n}_a + 1), \kappa_a(2\bar{n}_a + 1), 0, \gamma_b(2\bar{n}_b + 1)]$ is defined by $\langle \bar{n}_l(t)\bar{n}_k(t') + \bar{n}_k(t')\bar{n}_l(t) \rangle = 2\mathcal{D}_{lk}\delta(t - t')$.

D. Bipartite and tripartite entanglement

Once the matrix \mathcal{V} is obtained by solving Eq. (10), arbitrary bipartite entanglement can be quantified by the logarithmic negativity (LN) [115],

$$E_N \equiv \max[0, -\ln 2\eta^-] \quad (11)$$

with

$$\eta^- = 2^{-1/2}[\Sigma - (\Sigma^2 - 4\det\mathcal{V}_4)^{1/2}]^{1/2}, \quad (12)$$

where $\Sigma = \det\mathcal{A} + \det\mathcal{B} - 2\det\mathcal{C}$ and $\mathcal{V}_4 = \begin{pmatrix} \mathcal{A} & \mathcal{C} \\ \mathcal{C}^\top & \mathcal{B} \end{pmatrix}$ is the 4×4 block form of the correlation matrix, associated with two modes of interest [116]. \mathcal{A} , \mathcal{B} , and \mathcal{C} are the 2×2 blocks of \mathcal{V}_4 . $E_N > 0$ means that the interested two modes are entangled.

Additionally, tripartite entanglement among arbitrary three interested modes can also be studied by the function of the minimal residual contangle (MRC) [117, 118]:

$$\mathcal{R}_\tau \equiv \min \left[\mathcal{R}_\tau^{r|st}, \mathcal{R}_\tau^{s|rt}, \mathcal{R}_\tau^{t|rs} \right], \quad (13)$$

where

$$\mathcal{R}_\tau^{r|st} \equiv C_{r|st} - C_{r|s} - C_{r|t}, \quad (14)$$

with $C_{u|v}$ being the contangle of a subsystem of u and v (v contains one or two modes) and $\{r, s, t\} \in \{a, b, m_1, m_2\}$, is a proper entanglement monotone defined as the squared LN [117, 118]. $\mathcal{R}_\tau > 0$ indicates that the interested three modes are entangled.

III. OPTOMECHANICAL ENTANGLEMENT

In this part, we study the magnon-mediated optomechanical entanglement. To be more clear, we first re-examine the optomechanical entanglement without magnons, i.e., $g_1 = 0$ and $g_2 = 0$. Then we investigate the magnon-mediated optomechanical entanglement by taking a single sphere for example. Without loss of generality, we assume $g_1 = g_m \neq 0$ and $g_2 = 0$.

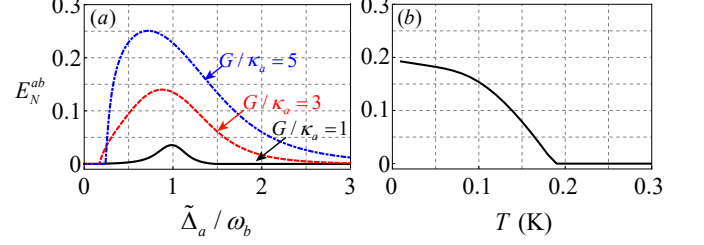


FIG. 2: (a) The optomechanical entanglement (E_N^{ab}) vs the normalized cavity detuning $\tilde{\Delta}_a / \omega_b$ with different optomechanical coupling strengths $G/\kappa_a = 1, 3, 5$ at the bath temperature $T = 20$ mK. (b) The LN E_N^{ab} vs the bath temperature T with the moderate optomechanical coupling strength $G/\kappa_a = 4$ and the frequency detuning $\tilde{\Delta}_a = 0.9\omega_b$. Other parameters are chosen as $\omega_a/2\pi = 10$ GHz, $\omega_b/2\pi = 10$ MHz, $\kappa_a/2\pi = 1$ MHz, $\gamma_b/2\pi = 100$ Hz.

A. Without magnons

When no spheres are placed in the cavity (i.e., $g_1 = g_2 = 0$), the proposed cavity-magnon optomechanics reduces to a standard optomechanical configuration comprising solely a cavity and a mechanical resonator. In this setup, optomechanical entanglement can be analyzed by plotting LN (E_N^{ab}) vs the normalized cavity detuning $\tilde{\Delta}_a / \omega_b$ with different linearized coupling strengths G in Fig. 2(a). Here, we employ experimentally accessible parameters[119, 120]: $\omega_a/2\pi = 10$ GHz, $\omega_b/2\pi = 10$ MHz, $\kappa_a/2\pi = 1$ MHz, $\gamma_b/2\pi = 10^2$ Hz, and $T = 20$ mK. Evidently, the optomechanical entanglement increases first and then decreases with the cavity detuning $\tilde{\Delta}_a / \omega_b$. Around $\tilde{\Delta}_a \approx \omega_b$, the optimal optomechanical entanglement is observed. By gradually increasing the optomechanical coupling, the optomechanical entanglement can be significantly enhanced (as depicted by the three curves). The generated optomechanical entanglement arises from both the two-mode squeezing effect ($a^\dagger b^\dagger + ab$, where $q \propto b + b^\dagger$) and the beam-splitter effect ($a^\dagger b + ab^\dagger$). While the former generates entanglement, and the latter cools the mechanical resonator to sustain the entanglement. In Fig. 2(b), the effect of the bath temperature on the optomechanical entanglement is further elucidated by fixing $\tilde{\Delta}_a = 0.9\omega_b$ and $G = 4\kappa_a$. It is shown that the optomechanical entanglement monotonically decreases as the bath temperature increases. The survival temperature for the optomechanical entanglement can be up to ~ 190 mK.

B. With magnons

To investigate the magnon-mediated optomechanical entanglement, we take the hybrid cavity-magnon optomechanics with a single sphere as an example, that is, we set $g_1 = g_m \neq 0$ and $g_2 = 0$ in Fig. 1. Correspondingly, $\Delta_1 = \Delta_m$ is specified. Within the framework

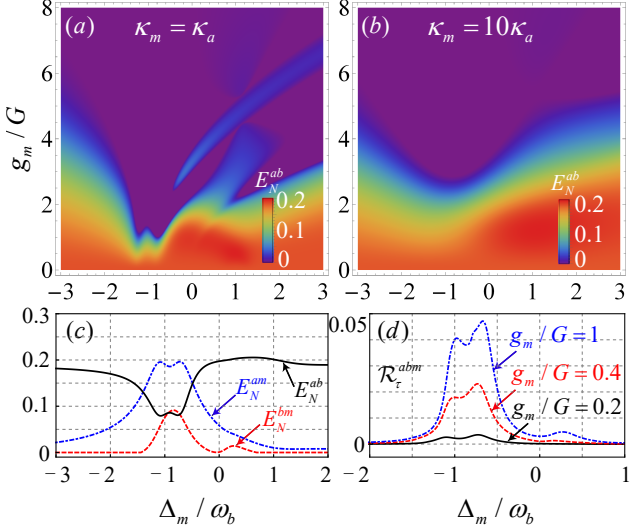


FIG. 3: Density plot of E_N^{ab} vs the normalized frequency detuning Δ_m/ω_b and the normalized magnon-photon coupling strength g_m/G with (a) $\kappa_m = \kappa_a$ and (b) $\kappa_m = 10\kappa_a$. (c) The optomechanical entanglement (E_N^{ab}), the magnon-photon entanglement (E_N^{am}), and the magnon-phonon entanglement (E_N^{bm}), vs the normalized magnon frequency detuning Δ_m/ω_b , where $g_m = G$ and $\kappa_m = \kappa_a$. (d) The magnon-photon-phonon entanglement (\mathcal{R}_τ^{abm}) VS the normalized magnon frequency detuning Δ_m/ω_b with different magnon-photon coupling strengths $g_m/G = 0.2, 0.4, 1$, where $\kappa_m = \kappa_a$ is taken. Other parameters are the same as those in Fig. 2(a) except for $G = 4\kappa_a$ and $\tilde{\Delta}_a = 0.9\omega_b$.

of cavity magnonics, the parameters such as the magnon frequency, the magnon-photon coupling, and the magnon decay rate are all tuned, leading to tunable optomechanical entanglement generated, as numerically investigated in Fig. 3. From Fig. 3(a), it is observed that the optomechanical entanglement decreases with increasing the magnon-photon coupling while keeping other system parameters fixed. Around $\Delta_m \approx \omega_b$, the optomechanical entanglement is optimal when g_m is comparable to G ($g_m \sim G$). This can also be evident in Fig. 3(b). Notably, a larger decay rate of the Kittle mode can significantly preserve the optomechanical entanglement, which can be given by comparing Figs. 3(a) and 3(b). Furthermore, Figure 3(c) elucidates that the optomechanical entanglement will be reduced when magnons are introduced. The reduction of the optomechanical entanglement is initially transformed into the magnon-photon entanglement (blue curve) and subsequently into the magnon-phonon entanglement (red curve). To simultaneously achieve these three entanglements, tuning the detuning of the cavity mode to be an optimal value is demanded. Additionally, we demonstrate that the magnon-photon-phonon tripartite entanglement (\mathcal{R}_τ^{abm}) around $\Delta_m \approx -\omega_b$ can be anticipated, as depicted in Fig. 3(d). By increasing the magnon-photon coupling, this tripartite entanglement noticeably improves, indicating that the optomechanical entanglement is also partially transferred to the tripartite

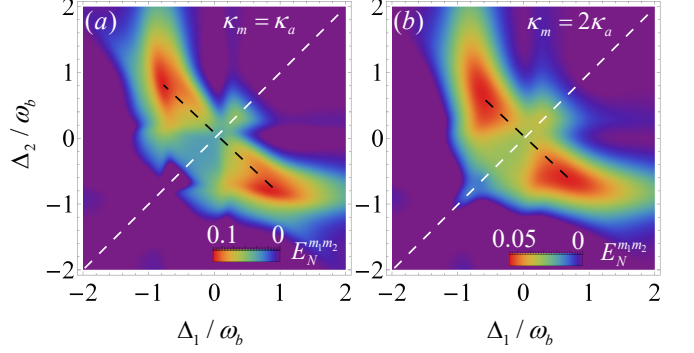


FIG. 4: Density plot of the magnon-magnon entanglement (E_N^{m1m2}) vs the normalized magnon frequency detunings Δ_1/ω_b and Δ_2/ω_b with (a) $\kappa_m = \kappa_a$ and (b) $\kappa_m = 2\kappa_a$. Other parameters are the same as those in Fig. 2(a) except for $g_m = G = 4\kappa_a$ and $\tilde{\Delta}_a = 0.9\omega_b$.

entanglement among the Kittle mode, the cavity mode, and the mechanical mode.

IV. MAGNON-MAGNON ENTANGLEMENT WITH THE OPTOMECHANICAL INTERFACE

Based on the aforementioned study of the optomechanical entanglement, it is evident that the optomechanical interface can serve as an effective entanglement generator. Therefore, we proceed to demonstrate the generation of magnon-magnon entanglement within the framework of two spheres included cavity-magnon optomechanics (see Fig. 1).

A. Magnon detuning effect

Figure 4 plots the magnon-magnon entanglement (E_N^{m1m2}) vs the normalized frequency detunings of two Kittle modes of the spheres with $\kappa_m = \kappa_a$ and $\kappa_m = 2\kappa_a$, where $g_m = G$ is fixed. The bat-shaped pattern in Fig. 4(a) demonstrates that the magnon-magnon entanglement can be symmetrically adjusted by varying the detunings of the Kittle modes. By varying one detuning while keeping the other unchanged, we observe that the magnon-magnon entanglement initially increases to its optimal value, and then decreases to zero. The optimal magnon-magnon entanglement can be predicted around $\Delta_1 = -\Delta_2 \approx \pm\omega_b$, which are symmetrically distributed on both sides of the white dashed line $\Delta_1 = \Delta_2$. The similar results are also evident from the bird-shaped pattern in Fig. 4(b). By comparing Figs. 4(a) and 4(b), we show that the larger magnon decay rate, the weaker magnon-magnon entanglement. Moreover, with increasing the magnon decay rate, the symmetric points about the diagonal line, where the optimal magnon-magnon entanglement is predicted, will converge in the case that magnons are resonant with the driving field, i.e., $\Delta_1 = \Delta_2 = 0$.

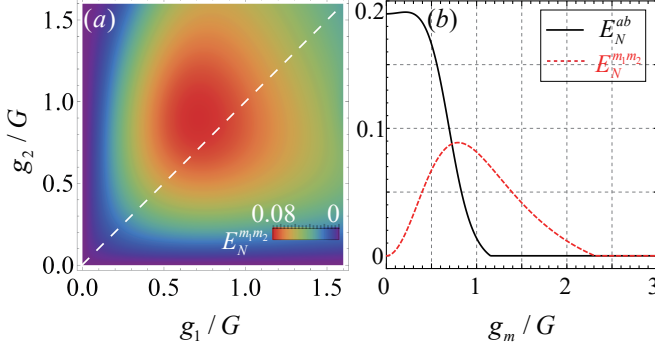


FIG. 5: (a) Density plot of the magnon-magnon entanglement ($E_N^{m_1 m_2}$) vs the normalized magnon-photon coupling strengths g_1/G and g_2/G . (b) The optomechanical entanglement (E_N^{ab}) and the magnon-magnon entanglement ($E_N^{m_1 m_2}$) vs the normalized magnon-photon coupling strength g_m/G . Other parameters are the same as those in Fig. 2(a) except for $\Delta_1 = -\omega_b$, $\Delta_2 = \omega_b$, $\kappa_m = \kappa_a$, $G = 4\kappa_a$ and $\tilde{\Delta}_a = 0.9\omega_b$.

B. Magnon-photon coupling effect

In this work, we assume that the magnons in the Kittle modes of two spheres have the identical coupling strength with the cavity mode. It is necessary to investigate the effect of two different coupling strengths g_1 and g_2 on the magnon-magnon entanglement generation. The numerical result is plotted in Fig. 5(a), where $\Delta_1 = -\omega_b$ and $\Delta_2 = \omega_b$ are fixed. Apparently, the optimal magnon-magnon entanglement can only be attained when two magnon-photon coupling strengths are comparable (see the white dashed line). With increasing the magnon-photon coupling strength, the magnon-magnon entanglement increases first to the optimal value, and then decreases to zero. To further show where the magnon-magnon entanglement comes, we plot the magnon-magnon entanglement ($E_N^{m_1 m_2}$) and the optomechanical entanglement (E_N^{ab}) vs the normalized coupling strength g_m/G in Fig. 5(b). We find that, with increasing the magnon-photon coupling to $g_m \sim G$, the optomechanical entanglement decreases to the optimal value of the magnon-magnon entanglement. By further increasing the magnon-photon coupling, both the magnon-magnon entanglement and the optomechanical entanglement reduce to zero. Obviously, the former decreases much slower than the latter. The behavior in Fig. 5(b) reveals that the magnon-magnon entanglement is partially transferred from the optomechanical entanglement.

C. Noise effect

In Fig. 6(a), the effects of the magnon decay rate on both the magnon-magnon and the optomechanical entanglement are investigated, where $g_m = G$ and $\Delta_1 = -\Delta_2 = -\omega_b$ are fixed. It is observed that larger decay rates of the magnons do not promote the genera-

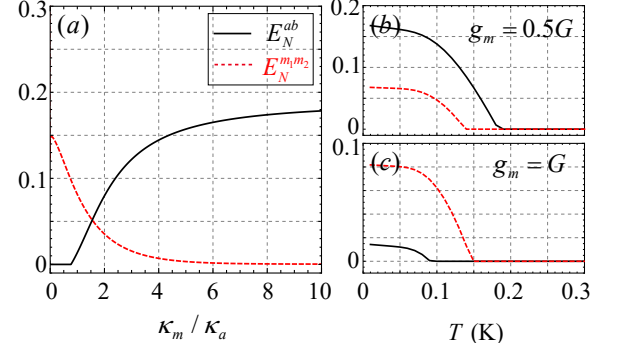


FIG. 6: The optomechanical entanglement (E_N^{ab}) and the magnon-magnon entanglement ($E_N^{m_1 m_2}$) vs (a) the normalized decay rate κ_m/κ_a , and the bath temperature T with (b) $g_m = 0.5G$ and (c) $g_m = G$. Here $\Delta_1 = -\omega_b$, $\Delta_2 = \omega_b$, $G = 4\kappa_a$, and $\tilde{\Delta}_a = 0.9\omega_b$ are fixed in (a-c). Other parameters are the same as those in Fig. 2(a) except for (a) $g_m = G$, (b,c) $\kappa_m = \kappa_a$.

tion of magnon-magnon entanglement. Instead, they facilitate the production of optomechanical entanglement, consistent with the findings from Figs. 3(a) and 3(b). This not only reveals that the entanglement exchange between these two entanglement occurs, but also shows that the generated magnon-magnon entanglement can be leveraged to restore the optomechanical entanglement by increasing the decay rate of the Kittle mode. Since the bath temperature is crucial for entanglement survival, we respectively plot $E_N^{m_1 m_2}$ and E_N^{ab} vs the bath temperature T in Figs. 6(b) and 6(c) with different magnon-photon coupling strengths, where $\kappa_m = \kappa_a$ is fixed. When the magnon-photon coupling strength is weaker than the optomechanical coupling strength [see $g_m = 0.5G$ in Fig. 6(b)], the optomechanical entanglement (the black curve) is stronger than the magnon-magnon entanglement (the red curve) within the survival temperature. But when the magnon-photon coupling strength is comparable with the optomechanical coupling strength [see $g_m = G$ Fig. 6(c)], the situation is reversed, that is, the magnon-magnon entanglement becomes much stronger than the optomechanical entanglement. Moreover, the survival temperature of the optomechanical entanglement is significantly shifted with varying the magnon-photon coupling. This indicates that the survival temperature of the magnon-magnon entanglement is more robust against the change of the magnon-photon coupling than that of the optomechanical entanglement.

V. MAGNON-BASED TRIPARTITE ENTANGLEMENT

Apart from the magnon-magnon entanglement, the optomechanical interface can also be used to produce tripartite entanglement, including the magnon-magnon-

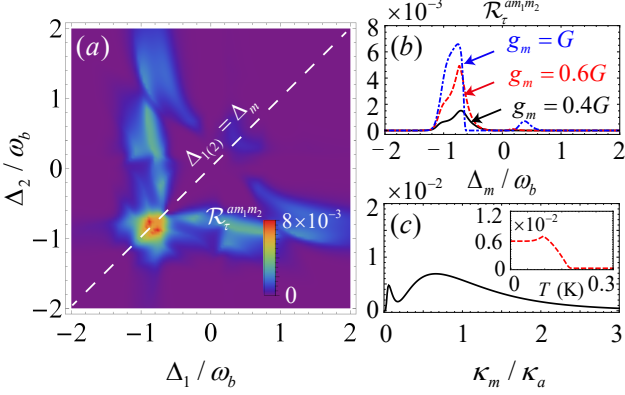


FIG. 7: (a) Density plot of the magnon-magnon-photon entanglement ($\mathcal{R}_\tau^{am_1m_2}$) vs the normalized frequency detunings Δ_1/ω_b and Δ_2/ω_b , where $g_m = G$, $\kappa_m = \kappa_a$, and $T = 20$ mK are taken. (b) The magnon-magnon-photon entanglement ($\mathcal{R}_\tau^{am_1m_2}$) vs the normalized frequency detuning Δ_m/ω_b with different magnon-photon coupling strengths $g_m/G = 0.4, 0.6, 1$, where $\kappa_m = \kappa_a$ and $T = 20$ mK. (c) The magnon-magnon-photon entanglement ($\mathcal{R}_\tau^{am_1m_2}$) vs the normalized decay rate κ_m/κ_a , where $g_m = G$ and $\Delta_1 = \Delta_2 = -\omega_b$. The plot of the magnon-magnon-photon entanglement vs the bath temperature is shown in the inset. Other parameters are the same as those in Fig. 2(a) except $G = 4\kappa_a$ and $\tilde{\Delta}_a = 0.9\omega_b$.

photon entanglement and the magnon-magnon-phonon entanglement, in hybrid cavity-magnon optomechanics.

A. Magnon-magnon-photon entanglement

In Fig. 7(a), we plot the magnon-magnon-photon entanglement ($\mathcal{R}_\tau^{am_1m_2}$) vs the normalized detunings Δ_1/ω_b and Δ_2/ω_b , where $g_m = G = 4\kappa_a$, $\kappa_m = \kappa_a$, and $T = 20$ mK. The eagle-pattern clearly indicates that the optimal magnon-magnon-photon entanglement is expected when magnons in two Kittle modes of the spheres are resonant and works on the blue-sideband, i.e., $\Delta_1 = \Delta_2 \approx -\omega_b$. When detunings deviate from this optimal point along the white diagonal line, where the resonant condition is maintained, we observe a rapid reduction in magnon-magnon-photon entanglement to zero. However, when nonidentical detunings are considered, this tripartite entanglement decreases slowly as detunings deviate from the optimal values, akin to a scenario where detunings stray from one of the eagle's wings. This indicates that nonidentical detunings can be used to protect this tripartite entanglement. Figure 7(b) demonstrates that the magnon-magnon-photon entanglement can be significantly enhanced by appropriately increasing the magnon-photon coupling strengths while varying the detuning $\Delta_m = \Delta_1 = \Delta_2$. Additionally, we observe that adjusting the magnon decay rate can also generate magnon-magnon-photon entanglement, as depicted in Fig. 7(c). The inset reveals the robustness of magnon-magnon-photon entanglement against the bath tempera-

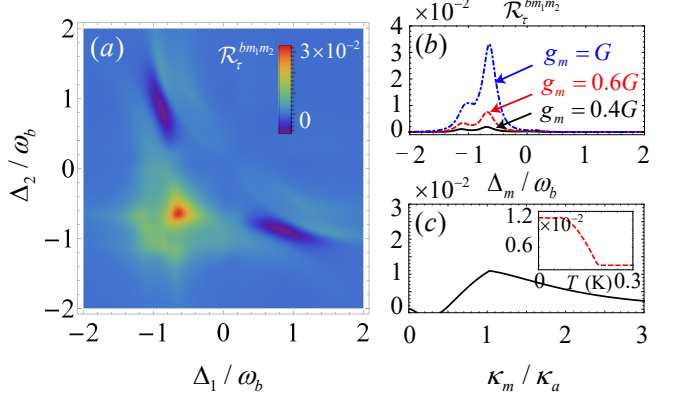


FIG. 8: (a) Density plot of the magnon-magnon-phonon entanglement ($\mathcal{R}_\tau^{bm_1m_2}$) vs the normalized frequency detunings Δ_1/ω_b and Δ_2/ω_b , where $g_m = G$, $\kappa_m = \kappa_a$, and $T = 20$ mK are taken. (b) The magnon-magnon-phonon entanglement ($\mathcal{R}_\tau^{bm_1m_2}$) vs the normalized frequency detuning Δ_m/ω_b with different magnon-photon coupling strengths $g_m/G = 0.4, 0.6, 1$, where $\kappa_m = \kappa_a$ and $T = 20$ mK. (c) The magnon-magnon-phonon entanglement ($\mathcal{R}_\tau^{bm_1m_2}$) vs the normalized decay rate κ_m/κ_a , where $g_m = G$ and $\Delta_1 = \Delta_2 = -\omega_b/2$. The plot of the magnon-magnon-phonon entanglement vs the bath temperature is shown in the inset. Other parameters are the same as those in Fig. 2(a) except $G = 4\kappa_a$ and $\tilde{\Delta}_a = 0.9\omega_b$.

ture when $T < 100$ mK. However, at a higher temperature, the entanglement diminishes and disappears around $T \approx 180$ mK.

B. Magnon-magnon-phonon entanglement

Next, we go on studying the magnon-magnon-phonon entanglement in the proposed hybrid cavity-magnon optomechanics. Note that there are no direct magnon-magnon and magnon-phonon couplings. We observe that optimal entanglement occurs around $\Delta_1 = \Delta_2 \approx -0.5\omega_b$. This point coincides with the nose of the fox-pattern depicted in Fig. 8(a). A comparison with Fig. 7(a) reveals that the magnon-magnon-phonon entanglement is stronger than that of magnon-magnon-photon entanglement, which can be regarded as that the mechanical mode can be cooled by the optomechanical beam-splitter interaction, or alternatively, the noise effect on the magnon-magnon-phonon entanglement is weaker than the magnon-magnon-photon entanglement because of the indirect interaction among magnons and phonons. We also find that such a tripartite entanglement can be improved by enhancing the magnon-photon coupling [see Fig. 8(b)]. Upon examining the entanglement with respect to the decay rate of the Kittle mode, we plot the magnon-magnon-phonon entanglement ($\mathcal{R}_\tau^{bm_1m_2}$) vs the normalized decay rate κ_m/κ_a . It is shown that a weaker decay rate does not benefit the generation of magnon-magnon-phonon entanglement.

By gradually increasing the decay rate, the magnon-magnon-phonon entanglement increases to its maximum and then decreases to zero. Comparing Figs. 7(c) and 8(c), we find that both the magnon-magnon-phonon entanglement and the magnon-magnon-photon entanglement have the similar resilience against the magnon decay rate. However, the magnon-magnon-phonon entanglement exhibits more robust against the bath temperature than that of the magnon-magnon-photon entanglement, as shown in the insets of Figs 7(c) and 8(c). In fact, the magnon-magnon-phonon entanglement is about two times than the magnon-magnon-photon entanglement within the survival temperature ~ 180 mK.

VI. CONCLUSION

In summary, we propose to generate diverse bipartite and tripartite entanglement in hybrid cavity-magnon optomechanics. Unlike standard cavity optomechan-

ics, our proposal not only enables magnon-mediated optomechanical entanglement but also allows for flexible magnon-magnon entanglement. It can even generate tripartite entanglement, including magnon-photophonon, magnon-magnon-photon, and magnon-magnon-phonon configurations. Moreover, optimal bipartite and tripartite entanglement can be achieved by tuning parameters. We further show that all entanglement can be enhanced via engineering the magnon-photon coupling, and are robust against the bath temperature within the survival temperature. In addition, we find that the optomechanical entanglement can be protected or restored by bad magnons with large decay rate, while other entanglement are significantly diminished. These findings suggest that our proposal offers a novel avenue to explore and control tunable macroscopic quantum effects in hybrid cavity-magnon optomechanics.

This work is supported by Zhejiang Provincial Natural Science Foundation of China under Grant No. LY24A040004.

[1] A. Prabhakar and D. D. Stancil, *Spin waves: Theory and applications* (Springer, 2009).

[2] C. Kittel, Phys. Rev. **110**, 836 (1958).

[3] B. Z. Rameshti, S. V. Kusminskiy, J. A. Haigh, K. Usami, D. Lachance-Quirion, Y. Nakamura, C.-M. Hu, H. X. Tang, G. E. Bauer, and Y. M. Blanter, Phys. Rep. **979**, 1 (2022).

[4] H. Yuan, Y. Cao, A. Kamra, R. A. Duine, and P. Yan, Phys. Rep. **965**, 1 (2022).

[5] S. Zheng, Z. Wang, Y. Wang, F. Sun, Q. He, P. Yan, and H. Yuan, J. Appl. Phys. **134**, 151101 (2023).

[6] Y. Li, W. Zhang, V. Tyberkevych, W.-K. Kwok, A. Hoffmann, and V. Novosad, J. Appl. Phys. **128**, 130902 (2020).

[7] D. Lachance-Quirion, Y. Tabuchi, A. Gloppe, K. Usami, and Y. Nakamura, Appl. Phys. Express **12**, 070101 (2019).

[8] X. Zuo, Z.-Y. Fan, H. Qian, M.-S. Ding, H. Tan, H. Xiong, and J. Li, arXiv preprint arXiv: 2310.19237 (2023).

[9] H. Huebl, C. W. Zollitsch, J. Lotze, F. Hocke, M. Greifenstein, A. Marx, R. Gross, and S. T. Goennenwein, Phys. Rev. Lett. **111**, 127003 (2013).

[10] Y. Tabuchi, S. Ishino, T. Ishikawa, R. Yamazaki, K. Usami, and Y. Nakamura, Phys. Rev. Lett. **113**, 083603 (2014).

[11] X. Zhang, C.-L. Zou, L. Jiang, and H. X. Tang, Phys. Rev. Lett. **113**, 156401 (2014).

[12] M. Goryachev, W. G. Farr, D. L. Creedon, Y. Fan, M. Kostylev, and M. E. Tobar, Phys. Rev. Appl. **2**, 054002 (2014).

[13] A. Ghirri, C. Bonizzoni, M. Maksutoglu, A. Mercurio, O. Di Stefano, S. Savasta, and M. Affronte, Phys. Rev. Appl. **20**, 024039 (2023).

[14] Y. Wang, Y. Zhang, C. Li, J. Wei, B. He, H. Xu, J. Xia, X. Luo, J. Li, J. Dong, W. He, Z. Yan, W. Yang, F. Ma, G. Chai, P. Yan, C. Wan, X. Han, and G. Yu, Nat. Commun. **15**, 2077 (2024).

[15] N. Kostylev, M. Goryachev, and M. E. Tobar, Appl. Phys. Lett. **108**, 062402 (2016).

[16] Y. Tabuchi, S. Ishino, A. Noguchi, T. Ishikawa, R. Yamazaki, K. Usami, and Y. Nakamura, Science **349**, 405 (2015).

[17] X. Zhang, C.-L. Zou, N. Zhu, F. Marquardt, L. Jiang, and H. X. Tang, Nat. Commun. **6**, 8914 (2015).

[18] Y.-P. Wang, G.-Q. Zhang, D. Zhang, X.-Q. Luo, W. Xiong, S.-P. Wang, T.-F. Li, C.-M. Hu, and J. You, Phys. Rev. B **94**, 224410 (2016).

[19] L. Bai, M. Harder, P. Hyde, Z. Zhang, C.-M. Hu, Y. Chen, and J. Q. Xiao, Phys. Phys. Lett. **118**, 217201 (2017).

[20] D. Zhang, X.-Q. Luo, Y.-P. Wang, T.-F. Li, and J. You, Nat. Commun. **8**, 1368 (2017).

[21] G.-Q. Zhang and J. You, Phys. Rev. B **99**, 054404 (2019).

[22] M. Harder, L. Bai, P. Hyde, and C.-M. Hu, Phys. Rev. B **95**, 214411 (2017).

[23] H. Liu, D. Sun, C. Zhang, M. Groesbeck, R. McLaughlin, and Z. V. Vardeny, Sci. Adv. **5**, aax9144 (2019).

[24] A. Mitridate, T. Trickle, Z. Zhang, and K. M. Zurek, Phys. Rev. D **102**, 095005 (2020).

[25] T. Ikeda, A. Ito, K. Miuchi, J. Soda, H. Kurashige, and Y. Shikano, Phys. Rev. D **105**, 102004 (2022).

[26] R. Barbieri, M. Cerdonio, G. Fiorentini, and S. Vitale, Phys. Lett. B **226**, 357 (1989).

[27] G. Liu, W. Xiong, and Z.-J. Ying, Phys. Rev. A **108**, 033704 (2023).

[28] Y.-P. Wang and C.-M. Hu, J. Appl. Phys. **127**, 130901 (2020).

[29] M. Harder, B. Yao, Y. Gui, and C.-M. Hu, J. Appl. Phys. **129**, 201101 (2021).

[30] W. Xiong, M. Tian, G.-Q. Zhang, and J. You, Phys. Rev. B **105**, 245310 (2022).

[31] W. Xiong, M. Wang, G.-Q. Zhang, and J. Chen, Phys.

Rev. A **107**, 033516 (2023).

[32] M. Tian, M. Wang, G.-Q. Zhang, H.-C. Li, and W. Xiong, arXiv preprint arXiv: 2304.13553 (2023).

[33] T. Neuman, D. S. Wang, and P. Narang, Phys. Rev. Lett. **125**, 247702 (2020).

[34] X.-L. Hei, P.-B. Li, X.-F. Pan, and F. Nori, Phys. Rev. Lett. **130**, 073602 (2023).

[35] M. Fukami, D. R. Candido, D. D. Awschalom, and M. E. Flatté, PRX Quantum **2**, 040314 (2021).

[36] B. Hetényi, A. Mook, J. Klinovaja, and D. Loss, Phys. Rev. B **106**, 235409 (2022).

[37] J. Li, S.-Y. Zhu, and G. Agarwal, Phys. Rev. Lett. **121**, 203601 (2018).

[38] Z. Zhang, M. O. Scully, and G. S. Agarwal, Phys. Rev. Res. **1**, 023021 (2019).

[39] J. Chen, X.-G. Fan, W. Xiong, D. Wang, and L. Ye, Phys. Rev. B **108**, 024105 (2023).

[40] J. Chen, X.-G. Fan, W. Xiong, D. Wang, and L. Ye, Phys. Rev. A **109**, 043512 (2024).

[41] H. Yuan, S. Zheng, Z. Ficek, Q. He, and M.-H. Yung, Phys. Rev. B **101**, 014419 (2020).

[42] J. Li and S.-Y. Zhu, New J Phys. **21**, 085001 (2019).

[43] F.-X. Sun, S.-S. Zheng, Y. Xiao, Q. Gong, Q. He, and K. Xia, Phys. Rev. Lett. **127**, 087203 (2021).

[44] Y.-L. Ren, J.-K. Xie, X.-K. Li, S.-L. Ma, and F.-L. Li, Phys. Rev. B **105**, 094422 (2022).

[45] D.-G. Lai, J.-Q. Liao, A. Miranowicz, and F. Nori, Phys. Rev. Lett. **129**, 063602 (2022).

[46] S. Haroche, Physics today **51**, 36 (1998).

[47] D. Bouwmeester, A. Ekert, and A. Zeilinger, *The Physics of Quantum Information* (Springer, Berlin, 2000).

[48] G. Adesso and F. Illuminati, Journal of Physics A: Mathematical and Theoretical **40**, 7821 (2007).

[49] M. Aspelmeyer, T. J. Kippenberg, and F. Marquardt, Rev. Mod. Phys. **86**, 1391 (2014).

[50] T. J. Kippenberg and K. J. Vahala, Opt. Express **15**, 17172 (2007).

[51] T. J. Kippenberg and K. J. Vahala, Science **321**, 1172 (2008).

[52] M. Metcalfe, Applied Physics Reviews **1**, 031105 (2014).

[53] Y.-C. Liu, Y.-W. Hu, C. W. Wong, and Y.-F. Xiao, Chin. Phys. B **22**, 114213 (2013).

[54] H. Chang and J. Zhang, Nanoscale **14**, 16710 (2022).

[55] S. Barzanjeh, A. Xuereb, S. Gröblacher, M. Paternostro, C. A. Regal, and E. M. Weig, Nat. Phys. **18**, 15 (2022).

[56] H. Xiong, L. Si, X. Lv, X. Yang, and Y. Wu, Science China Physics, Mechanics & Astronomy **58**, 1 (2015).

[57] D. Vitali, S. Gigan, A. Ferreira, H. Böhm, P. Tombesi, A. Guerreiro, V. Vedral, A. Zeilinger, and M. Aspelmeyer, Phys. Rev. Lett. **98**, 030405 (2007).

[58] A. K. Sarma, S. Chakraborty, and S. Kalita, AVS Quantum Science **3** (2021).

[59] B.-B. Li, L. Ou, Y. Lei, and Y.-C. Liu, Nanophotonics **10**, 2799 (2021).

[60] X. Liu, W. Liu, Z. Ren, Y. Ma, B. Dong, G. Zhou, and C. Lee, Int. J. Optomechatronics **15**, 120 (2021).

[61] A. Schliesser, G. Anetsberger, R. Rivière, O. Arcizet, and T. J. Kippenberg, New J. Phys. **10**, 095015 (2008).

[62] F. Marquardt, A. Clerk, and S. Girvin, J. Mod. Opt. **55**, 3329 (2008).

[63] N. T. Otterstrom, R. O. Behunin, E. A. Kittlaus, and P. T. Rakich, Phys. Rev. X **8**, 041034 (2018).

[64] J.-H. Gan, Y.-C. Liu, C. Lu, X. Wang, M. K. Tey, and L. You, Laser & Photonics Reviews **13**, 1900120 (2019).

[65] Y.-S. Park and H. Wang, Nat. Phys. **5**, 489 (2009).

[66] H. Xu, L. Jiang, A. Clerk, and J. Harris, Nature **568**, 65 (2019).

[67] Y.-C. Liu, Y.-F. Shen, Q. Gong, and Y.-F. Xiao, Phys. Rev. A **89**, 053821 (2014).

[68] J. Huang, D.-G. Lai, C. Liu, J.-F. Huang, F. Nori, and J.-Q. Liao, Phys. Rev. A **106**, 013526 (2022).

[69] C. Genes, D. Vitali, P. Tombesi, S. Gigan, and M. Aspelmeyer, Phys. Rev. A **77**, 033804 (2008).

[70] Y.-L. Zhang, C.-S. Yang, Z. Shen, C.-H. Dong, G.-C. Guo, C.-L. Zou, and X.-B. Zou, Phys. Rev. A **101**, 063836 (2020).

[71] A. Nunnenkamp, K. Børkje, J. Harris, and S. Girvin, Phys. Rev. A **82**, 021806 (2010).

[72] T. P. Purdy, P.-L. Yu, R. W. Peterson, N. S. Kampel, and C. A. Regal, Phys. Rev. X **3**, 031012 (2013).

[73] N. Aggarwal, T. J. Cullen, J. Cripe, G. D. Cole, R. Lanza, A. Libson, D. Follman, P. Heu, T. Corbitt, and N. Mavalvala, Nat. Phys. **16**, 784 (2020).

[74] A. Kronwald, F. Marquardt, and A. A. Clerk, New J. Phys. **16**, 063058 (2014).

[75] X.-Y. Lü, J.-Q. Liao, L. Tian, and F. Nori, Phys. Rev. A **91**, 013834 (2015).

[76] J.-Q. Liao and C. K. Law, Phys. Rev. A **83**, 033820 (2011).

[77] X.-Y. Lü, Y. Wu, J. Johansson, H. Jing, J. Zhang, and F. Nori, Phys. Rev. Letters **114**, 093602 (2015).

[78] L. Mercier de Lépinay, C. F. Ockeloen-Korppi, D. Malz, and M. A. Sillanpää, Phys. Rev. Lett. **125**, 023603 (2020).

[79] Z. Shen, Y.-L. Zhang, Y. Chen, Y.-F. Xiao, C.-L. Zou, G.-C. Guo, and C.-H. Dong, Phys. Rev. Lett. **130**, 013601 (2023).

[80] X. Xu, Y. Zhao, H. Wang, H. Jing, and A. Chen, Photon. Res. **8**, 143 (2020).

[81] N. Eshaqi-Sani, S. Zippilli, and D. Vitali, Phys. Rev. A **106**, 032606 (2022).

[82] M. Hafezi and P. Rabl, Opt. Express **20**, 7672 (2012).

[83] G. A. Peterson, F. Lecocq, K. Cicak, R. W. Simmonds, J. Aumentado, and J. D. Teufel, Phys. Rev. X **7**, 031001 (2017).

[84] M.-A. Miri, F. Ruesink, E. Verhagen, and A. Alù, Phys. Rev. Appl. **7**, 064014 (2017).

[85] Y.-F. Jiao, S.-D. Zhang, Y.-L. Zhang, A. Miranowicz, L.-M. Kuang, and H. Jing, Phys. Rev. Lett. **125**, 143605 (2020).

[86] X.-W. Xu, L. N. Song, Q. Zheng, Z. H. Wang, and Y. Li, Phys. Rev. A **98**, 063845 (2018).

[87] X.-B. Yan, Phys. Rev. A **101**, 043820 (2020).

[88] H. Lü, C. Wang, L. Yang, and H. Jing, Phys. Rev. Appl. **10**, 014006 (2018).

[89] A. Kronwald and F. Marquardt, Phys. Rev. Lett. **111**, 133601 (2013).

[90] C. Dong, V. Fiore, M. C. Kuzyk, and H. Wang, Phys. Rev. A **87**, 055802 (2013).

[91] X. Y. Zhang, Y. H. Zhou, Y. Q. Guo, and X. X. Yi, Phys. Rev. A **98**, 053802 (2018).

[92] D.-G. Lai, X. Wang, W. Qin, B.-P. Hou, F. Nori, and J.-Q. Liao, Phys. Rev. A **102**, 023707 (2020).

[93] M. Koppenhöfer, C. Padgett, J. V. Cady, V. Dharod, H. Oh, A. C. Bleszynski Jayich, and A. A. Clerk, Phys. Rev. Lett. **130**, 093603 (2023).

[94] M. Karuza, C. Biancofiore, M. Bawaj, C. Molinelli,

M. Galassi, R. Natali, P. Tombesi, G. Di Giuseppe, and D. Vitali, Phys. Rev. A **88**, 013804 (2013).

[95] Y. Liu, M. Davanço, V. Aksyuk, and K. Srinivasan, Phys. Rev. Lett. **110**, 223603 (2013).

[96] S. Weis, R. Rivière, S. Deléglise, E. Gavartin, O. Arcizet, A. Schliesser, and T. J. Kippenberg, Science **330**, 1520 (2010).

[97] W. Xiong, J. Chen, B. Fang, M. Wang, L. Ye, and J. Q. You, Phys. Rev. B **103**, 174106 (2021).

[98] X.-Y. Lü, W.-M. Zhang, S. Ashhab, Y. Wu, and F. Nori, Sci Rep **3**, 2943 (2013).

[99] J. Chen, Z. Li, X.-Q. Luo, W. Xiong, M. Wang, and H.-C. Li, Opt. Express **29**, 32639 (2021).

[100] W. Xiong, M. Wang, G.-Q. Zhang, and J. Chen, Phys. Rev. A **107**, 033516 (2023).

[101] Z. Shen, Y.-L. Zhang, Y. Chen, C.-L. Zou, Y.-F. Xiao, X.-B. Zou, F.-W. Sun, G.-C. Guo, and C.-H. Dong, Nat. Photon. **10**, 657 (2016).

[102] K. Fang, J. Luo, A. Metelmann, M. H. Matheny, F. Marquardt, A. A. Clerk, and O. Painter, Nat. Phys. **13**, 465 (2017).

[103] W. Xiong, D.-Y. Jin, Y. Qiu, C.-H. Lam, and J. Q. You, Phys. Rev. A **93**, 023844 (2016).

[104] O. Kyriienko, T. C. H. Liew, and I. A. Shelykh, Phys. Rev. Lett. **112**, 076402 (2014).

[105] E. A. Sete and H. Eleuch, Phys. Rev. A **85**, 043824 (2012).

[106] R. Ghobadi, A. R. Bahrampour, and C. Simon, Phys. Rev. A **84**, 033846 (2011).

[107] W. Xiong, Z. Li, G.-Q. Zhang, M. Wang, H.-C. Li, X.-Q. Luo, and J. Chen, Phys. Rev. A **106**, 033518 (2022).

[108] W. Xiong, Z. Li, Y. Song, J. Chen, G.-Q. Zhang, and M. Wang, Phys. Rev. A **104**, 063508 (2021).

[109] H. Jing, S. Özdemir, H. Lü, and F. Nori, Sci. Rep. **7**, 1 (2017).

[110] Z. Shen, G.-T. Xu, M. Zhang, Y.-L. Zhang, Y. Wang, C.-Z. Chai, C.-L. Zou, G.-C. Guo, and C.-H. Dong, Phys. Rev. Lett. **129**, 243601 (2022).

[111] Y.-P. Gao, C. Cao, T.-J. Wang, Y. Zhang, and C. Wang, Phys. Rev. A **96**, 023826 (2017).

[112] A. Hurwitz, *Selected Papers on Mathematical Trends in Control Theory*, edited by R. Bellman and R. Kalaba (Dover, New York, 1964).

[113] E. X. DeJesus and C. Kaufman, Phys. Rev. A **35**, 5288 (1987).

[114] P. C. Parks and V. Hahn, *Stability Theor* (Prentice Hall, New York, 1993).

[115] M. B. Plenio, Phys. Rev. Lett. **95**, 090503 (2005).

[116] R. Simon, Phys. Rev. Lett. **84**, 2726 (2000).

[117] G. Adesso and F. Illuminati, Journal of Physics A: Mathematical and Theoretical **40**, 7821 (2007).

[118] G. Adesso and F. Illuminati, New J Phys. **8**, 15 (2006).

[119] X. Zhang, C.-L. Zou, L. Jiang, and H. X. Tang, Sci. Adv. **2**, e1501286 (2016).

[120] D. Kleckner, W. Marshall, M. J. A. de Dood, K. N. Dinyari, B.-J. Pors, W. T. M. Irvine, and D. Bouwmeester, Phys. Rev. Lett. **96**, 173901 (2006).